METALS IN THE EXOSPHERE OF THE HIGHLY IRRADIATED PLANET WASP-12b[*]

L. Fossati[1], C. A. Haswell[1], C. S. Froning[2,14], L. Hebb[3], S. Holmes[1], U. Kolb[1], Ch. Helling[4], A. Carter[1], P. Wheatley[5],
A. C. Cameron[4], B. Loeillet[6,7], D. Pollacco[8], R. Street[9], H. C. Stempels[4,15], E. Simpson[8], S. Udry[10], Y. C. Joshi[8],
R. G. West[11], I. Skillen[12], and D. Wilson[13,16]

[1] Department of Physics and Astronomy, Open University, Walton Hall, Milton Keynes MK7 6AA, UK; l.fossati@open.ac.uk, C.A.Haswell@open.ac.uk,
s.holmes@open.ac.uk, U.C.Kolb@open.ac.uk, A.Carter@open.ac.uk
[2] Center for Astrophysics and Space Astronomy, University of Colorado, 593 UCB, Boulder, CO 80309-0593, USA; cynthia.froning@colorado.edu
[3] Department of Physics and Astronomy, Vanderbilt University, 6301 Stevenson Center Nashville, TN 37235, USA; leslie.hebb@vanderbilt.edu
[4] SUPA, School of Physics and Astronomy, University of St Andrews, North Haugh, St Andrews KY16 9SS, UK; Christiane.Helling@st-andrews.ac.uk,
acc4@st-andrews.ac.uk, Eric.Stempels@fysast.uu.se
[5] Department of Physics, University of Warwick, Coventry CV4 7AL, UK; p.j.wheatley@warwick.ac.uk
[6] Laboratoire d'Astrophysique de Marseille, BP 8, 13376 Marseille Cedex 12, France
[7] Université de Provence, CNRS (UMR 6110) and CNES, France; benoit.loeillet@oamp.fr
[8] Astrophysics Research Centre, School of Mathematics and Physics, Queen's University, University Road, Belfast BT7 1NN, UK; d.pollacco@qub.ac.uk,
esimpson05@qub.ac.uk, y.joshi@qub.ac.uk
[9] Las Cumbres Observatory, 6740 Cortona Drive, Suite 102, Santa Barbara, CA 93117, USA; rstreet@lcogt.net
[10] Observatoire de Genève, Université de Genève, 51 Ch. des Maillettes, 1290 Sauverny, Switzerland; Stephane.Udry@unige.ch
[11] Department of Physics and Astronomy, University of Leicester, Leicester, LE1 7RH, UK; rgw@astro.le.ac.uk
[12] Isaac Newton Group of Telescopes, Apartado de Correos 321, 38700 Santa Cruz de la Palma, Tenerife, Spain; wji@ing.iac.es
[13] Astrophysics Group, Keele University, Staffordshire, ST5 5BG, UK; david@davidmwilson.net

ABSTRACT

We present near-UV transmission spectroscopy of the highly irradiated transiting exoplanet WASP-12b, obtained with the Cosmic Origins Spectrograph on the *Hubble Space Telescope*. The spectra cover three distinct wavelength ranges: NUVA (2539–2580 Å), NUVB (2655–2696 Å), and NUVC (2770–2811 Å). Three independent methods all reveal enhanced transit depths attributable to absorption by resonance lines of metals in the exosphere of WASP-12b. Light curves of total counts in the NUVA and NUVC wavelength ranges show a detection at a 2.5σ level. We detect extra absorption in the Mg II $\lambda\lambda 2800$ resonance line cores at the 2.8σ level. The NUVA, NUVB, and NUVC light curves imply effective radii of $2.69 \pm 0.24\,R_J$, $2.18 \pm 0.18\,R_J$, and $2.66 \pm 0.22\,R_J$ respectively, suggesting the planet is surrounded by an absorbing cloud which overfills the Roche lobe. We detect enhanced transit depths at the wavelengths of resonance lines of neutral sodium, tin, and manganese, and at singly ionized ytterbium, scandium, manganese, aluminum, vanadium, and magnesium. We also find the statistically expected number of anomalous transit depths at wavelengths not associated with any known resonance line. Our data are limited by photon noise, but taken as a whole the results are strong evidence for an extended absorbing exosphere surrounding the planet. The NUVA data exhibit an early ingress, contrary to model expectations; we speculate this could be due to the presence of a disk of previously stripped material.

Key words: stars: individual (WASP-12)

1. INTRODUCTION

Observations of the transiting extrasolar planets HD209458b and HD189733b revealed an enhanced transit depth at the wavelengths of several UV resonance lines (Vidal-Madjar et al. 2003, 2004; Lecavelier des Etangs et al. 2010). These UV lines from the ground state are sensitive probes of the presence of atomic and ionic species. Their presence enhanced the effective radius of the planet during transit, implying the planet is surrounded by an extended cloud of size comparable to or larger than its Roche lobe (Vidal-Madjar et al. 2003, 2004; Ben-Jaffel 2007; Vidal-Madjar et al. 2008). This was attributed

to a hydrodynamic "blow-off" of the planet's outer atmosphere caused by the intense irradiation suffered by this hot Jupiter exoplanet. An alternative explanation in which the planet is surrounded by a cloud of energetic neutral atoms caused by interactions with the host star's stellar wind has, however, been suggested (Holmström et al. 2009; Ekenbäck et al. 2010). WASP-12b is one of the hottest and most irradiated transiting exoplanets and orbits extremely close to a late F-type host star (Hebb et al. 2009). WASP-12b is, therefore, an attractive target to explore the properties of the phenomenon observed in HD209458b, and might yield evidence distinguishing between the suggested underlying causes.

The initial UV observations of HD209458b were in the far-UV around the Lyα emission line. The abundance of hydrogen makes this an attractive line to observe, but the temporal and spatial variability of stellar Lyα emission is a highly undesirable complicating factor. For this reason, and to obtain better signal to noise, we observed WASP-12 in the near-UV where there are many other resonance lines (Morton 1991, 2000), including the very strong Mg II UV resonance lines. This work became possible with the installation of the

Table 1
Limits Adopted to Define the Analyzed Wavelength Regions Around the Mg II Resonance Lines

Band	Wavelength Range (Å)	Band	Wavelength Range (Å)	Band	Wavelength Range (Å)
n_b	2782.75–2795	m_b	2782.75–2787.5	w_b	2782.75–2783.75
n_r	2805–2817.25	m_r	2812.5–2817.25	w_r	2816.25–2817.25
n_c	2795–2805	m_c	2787.5–2812.5	w_c	2783.75–2816.25

Cosmic Origins Spectrograph (COS) on the *Hubble Space Telescope* (*HST*) reinstating and enhancing our capabilities for UV spectroscopy.

2. OBSERVATIONS AND DATA REDUCTION

The planet-hosting star WASP-12 was observed for five consecutive *HST* orbits on 2009 September 24th and 25th with COS; see Green et al. (2003, 2010), and Osterman et al. (2010) for details of COS. We used the NUV G285M grating at the 2676 Å setting, which provides non-contiguous spectra over three wavelength ranges (NUVA: 2539–2580 Å; NUVB: 2655–2696 Å; NUVC: 2770–2811 Å) at a spectral resolution of $R \sim 20{,}000$, in TIME-TAG mode. The exposure time was 2334 s in the first *HST* orbit and about 3000 s per subsequent *HST* orbit. The optical ephemeris gives ingress during the second *HST* orbit and egress in the fourth *HST* orbit.

We downloaded data from MAST[17] adopting CALCOS V.2.11b[18] for calibration. Despite the early date of our observations, the CALCOS reference files used were at a fairly mature stage for the near-UV (NUV) data. In particular, the flat field had been updated to its flight version. In our time series analysis we used the count rates obtained after background subtraction, rather than the flux calibrated spectra. The high-quality flat field and the relatively low background of the NUV channel mean the uncertainties are dominated by poisson statistics. The count rates summed over wavelength are roughly 10 count s^{-1}, 28 count s^{-1}, and 13 count s^{-1}, respectively, for the NUVA, NUVB, and NUVC ranges. The resulting signal-to-noise ratio per pixel in the NUVB spectrum is $\sim$10 for each 3000 s exposure.

Figure 1 shows the total summed spectrum in comparison with synthetic fluxes from the LLMODELS stellar model atmosphere code (Shulyak et al. 2004), assuming the fundamental parameters and metallicity given by Hebb et al. (2009). We used the VALD database (Piskunov et al. 1995; Kupka et al. 1999; Ryabchikova et al. 1999) for atomic line parameters and SYNTH3 (Kochukhov 2007) for spectral synthesis. All three regions are strongly affected by many blended photospheric absorption lines; we observe no unabsorbed stellar continuum. The NUVB region is closest to the continuum, while the NUVC region is strongly absorbed by the Mg II doublet at 2795.5 Å and 2802.7 Å.

3. DETECTION OF A WAVELENGTH-DEPENDENT PLANET TRANSIT

We expect the planet's atmosphere to absorb particularly in the resonance lines of abundant elements. We used three
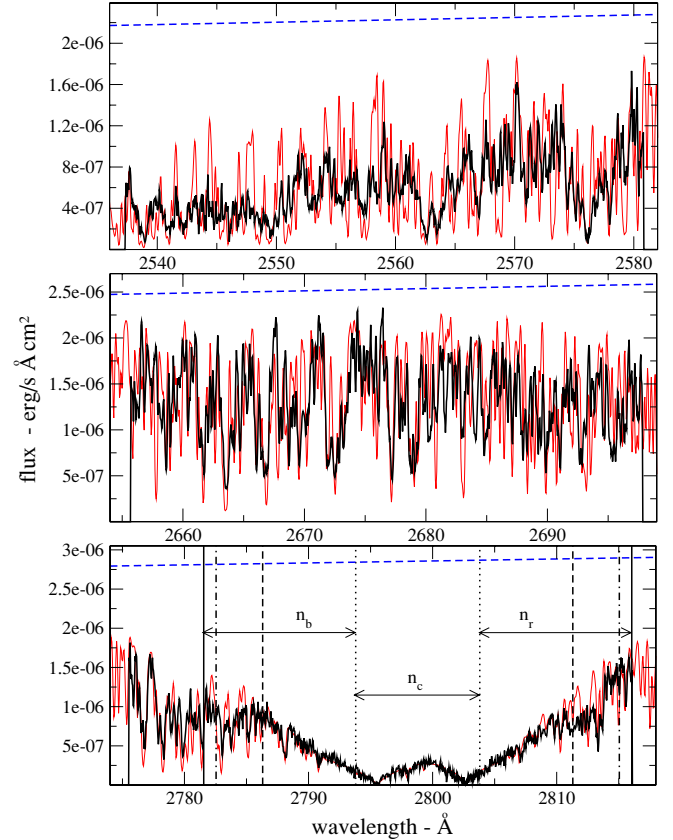
Figure 1. Comparison between the observed mean spectrum of WASP-12 (thick black line) and LLMODELS synthetic fluxes (thin red line). The blue dashed line shows the modeled level of the stellar continuum flux. The three observed spectral ranges are defined as NUVA, NUVB, and NUVC from top to bottom. In the bottom panel, the vertical lines show the limits applied for the wavelength regions, in laboratory wavelengths, accounted for producing the photometric indexes described in Section 3.1, showing as example the wavelength regions of n_b, n_c, and n_r.

methods to examine the data for wavelength dependence of the transit light curve.

3.1. The Mg II Lines

The most prominent observed lines in the stellar photosphere are the Mg II lines, and we might expect these strong lines to be detectable in the planet's atmosphere too. We adopted the method pioneered by Charbonneau et al. (2002) in their detection of the sodium D lines in the atmosphere of HD209458b. We divided the NUVC data, which are centered on the Mg II resonance lines, into "blue" (b), "red" (r), and "center" (c) spectral regions. We tried three different widths of the center band, "narrow" (n), "medium" (m), and "wide" (w); see Figure 1 and Table 1. For each of these bands, we produced a photometric time series and the associated uncertainty based on Poisson statistics. Each photometric index was obtained by summing the observed counts over the given wavelength range. In this way

"$n_b(t)$" indicates the count rate in the blue side "narrow" set at the time t.

The stellar limb darkening could potentially cause a color-dependent transit shape (e.g., Brown et al. 2001). To assess this, we calculated the difference of the blue and red spectral regions for the "n," "m," and "w" bands as a function of time (see Equation (1) of Charbonneau et al. 2002). We looked for variations in the transit depth due to the stellar limb darkening calculating the difference between the mean photometric indexes obtained in- and out-of-transit (see Equation (2) of Charbonneau et al. 2002). All values we obtained were clearly consistent with no variation.

To examine time dependence using Charbonneau et al. (2002)'s method, we calculated in each band ("n," "m," and "w") the difference between the light curve of the central band and the mean light curve of the blue and red bands:

$$
\begin{aligned}
n_{Mg}(t) &= n_c(t) - [n_b(t) + n_r(t)] / 2 \\
m_{Mg}(t) &= m_c(t) - [m_b(t) + m_r(t)] / 2 \\
w_{Mg}(t) &= w_c(t) - [w_b(t) + w_r(t)] / 2.
\end{aligned} \quad (1)
$$

In this way, we removed any limb darkening dependence. Again, the time series have rms scatter consistent with photon noise: $(\sigma[n_{Mg}(t_{out})] \sim \sigma[m_{Mg}(t_{out})] \sim \sigma[w_{Mg}(t_{out})] \sim 3.4 \times 10^{-3}$ count s^{-1}). We then calculated the difference between the mean in-transit and out-of-transit flux:

$$
\begin{aligned}
\Delta n_{Mg} &= \overline{n_{Mg}(t_{in})} - \overline{n_{Mg}(t_{out})} \\
&= (3.5 \pm 4.1) \times 10^{-3} \text{ count s}^{-1} \\
\Delta m_{Mg} &= \overline{m_{Mg}(t_{in})} - \overline{m_{Mg}(t_{out})} \\
&= (-4.7 \pm 4.1) \times 10^{-3} \text{ count s}^{-1} \\
\Delta w_{Mg} &= \overline{w_{Mg}(t_{in})} - \overline{w_{Mg}(t_{out})} \\
&= (-11.4 \pm 4.1) \times 10^{-3} \text{ count s}^{-1}.
\end{aligned} \quad (2)
$$

These results show the detection of a deeper transit in the "m" and "w" bands at 1.1σ and 2.8σ, respectively. Since the value obtained in the "n" band is comparable to the resulting photon noise error bar, we believe that the non-detection is due to the very low signal level in n_c along with absorption occurring in the wide n_r and n_b bands. The size and the significance of the detection increase as the signal included in the center band increases, just as we would expect if the enhanced transit depth in the Mg II doublet is genuine.

3.2. The Transit Light Curve

We compared the light curves obtained for each observed wavelength range and the one calculated from visible photometry, as shown in Figure 2.

The NUVB wavelength range is the closest to the continuum and shows a transit depth that matches, at $\sim 1\sigma$, the transit light curve derived by Hebb et al. (2009) from optical photometry. In the NUVA and NUVC wavelength ranges, we obtained a deeper transit at about 2.5σ level. These three light curves were normalized to the line passing through the out-of-transit photometric points (first and fifth exposures). The slopes of the three normalization lines are 3.8×10^{-3} for the NUVA region, 3.3×10^{-2} for the NUVB region, and 1.0×10^{-2} for the NUVC region. These values are small enough that the applied normalization did not change the transit shape.

The NUVC spectral region is clearly dominated by the Mg II resonance lines that are likely to be responsible for the detected extra depth in the transit light curve. The NUVA spectral region
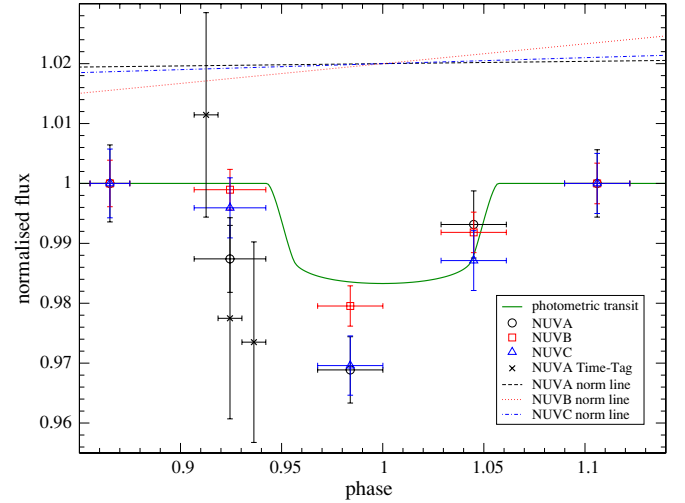

Figure 2. Light curve obtained for each observed wavelength range (NUVA: open black circles; NUVB: open red squares; NUVC: open blue triangles). The horizontal error bar defines the orbital phase range covered by each observation. The vertical uncertainty comes from a Poissonian treatment of the error bars. The full green line shows the MCMC fit to the optical transit light curve (Hebb et al. 2009). The black crosses show the NUVA spectral range split into three equally exposed sub-exposures. Lines indicate the normalization gradient applied.

includes resonance lines of Na I, Al I, Sc II, Mn II, Fe I, and Co I (Morton 1991, 2000). The stellar spectrum is dominated by Mg I and Fe I lines coming from low-energy levels. Probably, these spectral features, likely to be present also in the spectrum of the planet atmosphere, produce the observed deeper transit (see Vidal-Madjar et al. 2004, for a similar case).

The end of the second exposure is at the phase of the planet ingress, as shown in Figure 2. It is notable that the NUVA flux during the second exposure lies below the out-of-transit level by $\sim 2\sigma$. We divided this particular exposure into three equal sub-exposures plotted as black crosses. These suggest an early ingress in the NUVA spectral region.

3.3. Detection of Other Elements

In each of the three observed wavelength ranges we calculated a ratio spectrum (d_λ) between the in-transit spectrum (in$_\lambda$) measured in the third exposure and the out-of-transit spectrum (out$_\lambda$), the mean of the first and fifth exposures. With these ratio spectra we associated two different uncertainties: (1) the standard deviation from the mean, $\bar{d}$, which we denote as $\sigma_{d_\lambda|\text{exp}}$. (2) The uncertainty for each individual wavelength point in the ratio spectrum from the propagated uncertainties. We denote this as $\sigma_{d_\lambda|\text{prop}}$. Expressed symbolically:

$$
d_\lambda = \frac{\text{in}_\lambda}{\text{out}_\lambda} \quad (3)
$$

and

$$
\sigma_{d_\lambda|\text{exp}} = \frac{\sqrt{(\bar{d} - d_\lambda)^2}}{N - 1} \quad \sigma_{d_\lambda|\text{prop}} = \sqrt{\left(\frac{\sigma_{\text{in}_\lambda}}{\text{out}_\lambda}\right)^2 + \left(\frac{\text{in}_\lambda \sigma_{\text{out}_\lambda}}{\text{out}_\lambda^2}\right)^2}, \quad (4)
$$

where N is the number of points, $\sigma_{\text{in}_\lambda} = \sqrt{\text{in}_\lambda}$, and $\sigma_{\text{out}_\lambda} = \sqrt{\text{out}_\lambda}$. In NUVA, NUVB, and NUVC $\sigma_{d_\lambda|\text{exp}}$ is 0.34, 0.12, and 0.76, respectively. $\sigma_{d_\lambda|\text{prop}}$ varies with wavelength, as shown in Figure 3.

Table 2 lists the wavelength points of d_λ (in laboratory wavelengths) with deviations of more than 3σ from $\bar{d}$, assuming

Table 2
Wavelength of the Spectral Points Deviating More Than 3σ, Adopting Two Different σs: $\sigma_{d_\lambda|exp}$ and $\sigma_{d_\lambda|prop}$

Wavelength $\lambda - 2500$ Å $3\times\sigma_{d_i|exp}$	Resonance Line Å $3\times\sigma_{d_i|prop}$	Wavelength $\lambda - 2500$ Å $3\times\sigma_{d_i|prop}$	Resonance Line Å	Wavelength $\lambda - 2600$ Å $3\times\sigma_{d_i|exp}$	Resonance Line Å	Wavelength $\lambda - 2000$ Å $3\times\sigma_{d_i|exp}$	Resonance Line Å	Wavelength $\lambda - 2000$ Å $3\times\sigma_{d_i|prop}$	Resonance Line Å
		NUVA: ~2531–2586			NUVB: ~2650–2703			NUVC: ~2770–2821	
38.719	YbII@38.662			63.424				793.234#	MgII@795.528
38.806				63.549#				793.793#	MgII@795.528
39.021				63.674#				793.833#	MgII@795.528
		40.703#	ScII@40.822	66.633#				793.993#	MgII@795.528
		40.833	ScII@40.822	69.714	AlII@69.155*			794.353#	MgII@795.528
40.876	ScII@40.822	40.876#	ScII@40.822	72.459	VII@72.007*	795.272#	MgII@795.528		
41.048#				72.751#	VII@72.007*	795.391#	MgII@795.528		
		41.135#		78.732#	VII@78.575*	795.431#	MgII@795.528		
		41.178#		83.003#	VII@83.090	795.511#	MgII@795.528		
		42.126#		89.792	VII@89.884*	795.551#	MgII@795.528		
		43.893#	NaI@43.840	97.927#		795.591#	MgII@795.528		
		43.893#	NaI@43.872			795.631#	MgII@795.528		
		45.960#				795.711#	MgII@795.528		
46.175#	SnI@46.548*	46.175#	SnI@46.548*						
		46.691#	SnI@46.548*					795.911#	MgII@795.528
		48.369#	EuIII@48.583*					796.110#	MgII@795.528
		49.402#						796.150	MgII@795.528
		49.445#						796.629#	MgII@795.528
		50.004#						796.869	MgII@795.528
62.363#								796.909#	MgII@795.528
		62.535#						797.468#	MgII@795.528
		62.620#						797.907#	MgII@795.528
		63.348#	ScII@63.190*			797.947	MnI@798.269*		
63.391#	ScII@63.190*					801.059#	MnI@801.082		
63.477	ScII@63.190*							801.697#	MgII@802.705
		63.563	ScII@63.190*			802.375#	MgII@802.705		
75.999#	MnII@76.106					802.415#	MgII@802.705		
76.085#	MnII@76.106					802.495#	MgII@802.705		
76.127#	MnII@76.106					802.614	MgII@802.705		
								802.734#	MgII@802.705
								804.049#	MgII@802.705
								816.182#	

Notes. For each detected deviating point, we show the resonance line found lying at the same position or close to it (*). In the NUVB region, we did not detect any deviating point assuming $\sigma = \sigma_{d_\lambda|prop}$. The deviating points marked with a **#** deviate by $\geqslant 3.5\sigma$ from the mean.
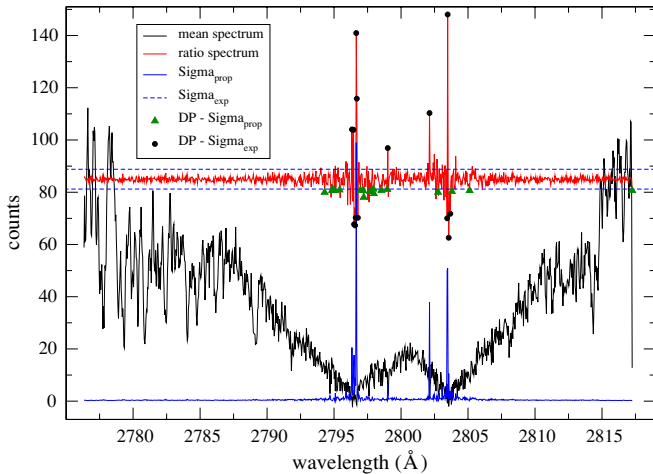

Figure 3. Black line shows the observed spectrum obtained averaging the five available COS spectra. The red line shows the d_λ spectrum, magnified five times and shifted upward for display reasons. The blue lines show the $\sigma_{d_\lambda|prop}$ spectrum (full line) and the values of $\sigma_{d_\lambda|exp}$ (dashed lines). The full black circles show the position of the deviating points assuming $\sigma = \sigma_{d_\lambda|exp}$, while the full green triangles show the position of the deviating points assuming $\sigma = \sigma_{d_\lambda|prop}$.

both $\sigma = \sigma_{d_\lambda|exp}$ (left column) and $\sigma = \sigma_{d_\lambda|prop}$ (right column). Assuming a Gaussian distribution and having $N = 1024 \times 3$ wavelength points, we expect nine points in the d_λ array to fall outside 3σ from the mean. Since the number of detected deviating wavelength points is much larger than nine we looked for correspondences with resonance lines (Morton 1991, 2000). Table 2 lists the deviating wavelength points and the corresponding resonance lines. We include occurrences of resonance lines within a few km s^{-1} of a deviating wavelength point, for example, the Sc II line at 2563.190 Å.

In the NUVA wavelength region and adopting $\sigma = \sigma_{d_\lambda|exp}$ we obtained 3σ deviations corresponding to the position of three resonance lines: Yb II at 2538.662 Å, Sc II at 2540.822 Å, and Mn II at 2576.106 Å. Assuming instead $\sigma = \sigma_{d_\lambda|prop}$ Sc II at 2540.822 Å and the Na II doublet at 2543.8 Å are picked out. In the NUVB region, we only find the V II line at 2683.090 Å and only assuming $\sigma = \sigma_{d_\lambda|exp}$. However three other V II resonance lines and an Al II line lie close to other detected deviating points. In the NUVC region, we recognize immediately that most of the deviating points are in the core of the Mg II resonance lines, both assuming $\sigma = \sigma_{d_\lambda|exp}$ and $\sigma = \sigma_{d_\lambda|prop}$. We also pick out the Mn I line at 2801.082 Å, while the Mn I line at 2798.269 Å lies close to the wavelength of another deviating point.

Figure 3 shows the cores of the Mg II resonance lines. We show the observed spectrum, d_λ, $\sigma_{d_\lambda|prop}$, and the deviating wavelength points both assuming $\sigma = \sigma_{d_\lambda|exp}$ and $\sigma = \sigma_{d_\lambda|prop}$. With $\sigma = \sigma_{d_\lambda|exp}$ the deviating points correspond to the core

of the Mg II line where the signal level is low. This is to be expected: the low count rates at these wavelengths lead d_λ to be very noisy here. In contrast, with $\sigma = \sigma_{d_\lambda|\text{prop}}$ each element of the d_λ spectrum is assessed against its own Poisson error. In this case, the deviating points are all below the mean rate spectrum, and the deviating points appear at the margins of the line core. These points indicate excess Mg II absorption during transit. This is attributable to absorption by the planet's atmosphere. This pattern is seen not only for the two Mg II resonance lines, but also for the Sc II line at 2563.190 Å. This line, together with the Mn I line at 2798.269 Å, has the intriguing property that the difference between the position of the resonance line and of the detected deviating wavelength point(s) corresponds to a velocity of $\sim$30 km s^{-1} (about three resolution elements), close to the planet escape velocity of $\sim$37 km s^{-1} (Hebb et al. 2009), although it would not then be clear why this pattern does not appear also for other detected lines of the same ion.

There are 95 known resonance lines lying within the observed wavelength ranges, including those of heavy elements. This is a small minority of the more than 4000 lines present in the stellar spectrum. The fact that we find deviating points predominantly at wavelengths corresponding to resonance lines strongly suggests we are detecting features produced by the planet atmosphere. Reassuringly, with either definition of σ, we obtained nine points that do not match any known resonance line, in perfect accordance with statistical expectations. We repeated the exercise picking out deviations in excess of 3.5σ, obtaining almost the same deviating points at the position of known resonance lines and fewer points where no resonance lines were found.

4. DISCUSSION

We have performed three independent analyses, each of which suggests absorption in the resonance lines of metals from an extended atmosphere surrounding the transiting planet WASP-12b. In Section 3.1, we found a deeper transit in the core region of the Mg II doublet at the 2.8σ level.

In Section 3.2, the transit depths in the NUVA, NUVB, and NUVC wavelength ranges respectively imply effective planet radii of 2.69 $\pm$ 0.24 R_J, 2.18 $\pm$ 0.18 R_J, and 2.66 $\pm$ 0.22 R_J. WASP-12b's optical radius is $R_P = 1.79 \pm 0.09 \, R_J$, while the mean Roche lobe radius is 2.36 R_J using Paczyński's (1971) prescription.

Table 2 shows that we detect enhanced transit depths at the wavelengths of resonance lines of neutral sodium, tin and manganese, and at singly ionized ytterbium, scandium, manganese, aluminum, vanadium, and magnesium. Finally, we detect an enhanced transit depth within 0.12 Å of a resonance line of doubly ionized europium. We also find the statistically expected number of anomalous transit depths at wavelengths not associated with any known resonance line.

Taken as a whole, these results constitute compelling evidence that WASP-12b is surrounded by an exosphere which over-fills the planet's Roche lobe, confirming predictions by Li et al. (2010). This exosphere is likely composed of a number of elements/ions, including probably Na I, Mg I, Mg II, Al I, Sc II, Mn II, Fe I, and Co I. The phenomenon found in HD209458b (Vidal-Madjar et al. 2003, 2008) probably occurs generally for hot Jupiter exoplanets. By analogy with HD209458b, and as WASP-12b and its host star are almost certainly predominantly composed of hydrogen, we expect that this exosphere is hydrogen rich.

Models by Yelle (2004) suggest that elements other than H and He should not be present in the upper atmosphere due to the low vertical mixing rate, but this takes Jupiter as the starting point. WASP-12b is extremely close to the host star and consequently the stellar irradiation and tidal effects could induce prodigious mixing, affecting the chemistry of the planet atmosphere. Our detections of several metallic elements and/or ions are certainly consistent with a metal-rich atmosphere for WASP-12b.

The most surprising result is provided by the juxtaposition of our data with the optical ephemeris. We took contemporaneous optical photometry with OU-OAM PIRATE[19] which showed the ephemeris of Hebb et al. (2009) remains accurate. Figure 2 shows the NUVA transit has an early ingress and an egress consistent with the optical ephemeris. In contrast, naive momentum considerations and hydrodynamic simulations would instead suggest that the effect of a diffuse cloud surrounding the planet would be to smear and delay egress while ingress is relatively unaffected, see, e.g., Figures 1 and 2 of Schneiter et al. (2007).

In detail, the shape of the diffuse cloud may well be element/ion dependent since different elements/ions behave differently in the presence of strong radiation pressure. This can explain why we observe different transit shapes in the NUVA region and the other regions. As Figure 1 shows, the stellar spectrum in the NUVA region is strongly absorbed by a plethora of lines, dominated by those of neutral elements. The NUVC region is also strongly absorbed in the stellar photosphere but predominantly from the Mg II doublet. It is presumably the cumulative absorption from many relatively weak spectral lines in the planet's exosphere which creates the excess transit depth in the NUVA region, while Table 2 and Equation (2) demonstrate that planet's absorption in the NUVC region is associated with the Mg II doublet. The Mg II ion will experience different forces to neutral atoms in an environment where there is certainly a strong radiation field, and strong and varying large-scale magnetic fields are also likely. The NUVB light curve is least deviant from the optical transit, and this is consistent with the relative dearth of strongly absorbing lines in this spectral window, see Figure 1.

We do not have any detailed explanation for the observed early ingress in NUVA, but we speculate the effect could be produced if material is lost from the planet exosphere and forms a diffuse ring or torus around the star enveloping the planet's orbital path, as models suggest (Li et al. 2010). The orbital motion of the planet through this medium might compress the material in front of it. This could increase the opacity of the medium through which the star is viewed immediately before first contact. A void in the medium might be expected to form behind the planet, and consequently the egress is relatively unaffected by the diffuse ring.

Our observations demonstrate that COS spectroscopy of transiting exoplanets has the potential to detect many species via transmission spectroscopy, and to measure velocities and deduce spatial distributions. There are now about 40 known transiting exoplanets with orbital periods shorter than that of HD209458b. Many of these transit stars are significantly brighter than WASP-12b. COS spectroscopy of brighter examples will allow us to probe the exosphere species-by-species examining their density, velocity, and spatial distributions. This detailed information should allow us to determine whether these planets really

---

[19] http://pirate.open.ac.uk

are being photo-evaporated by their host stars, and, if so, to empirically deduce the mass loss rate. We encourage detailed element/ion-dependent modeling of the exosphere in the highly irradiated environment of WASP-12b and similar systems, and observations of other similar extrasolar planets. There is a rich new parameter space to explore.

Facilities: HST (COS).

REFERENCES

Ben-Jaffel, L. 2007, ApJ, 671, L61
Brown, T. M., Charbonneau, D., Gilliland, R. L., Noyes, R. W., & Burrows, A. 2001, ApJ, 552, 699
Charbonneau, D., Brown, T. M., Noyes, R. W., & Gilliland, R. L. 2002, ApJ, 568, 377
Ekenbäck, A., et al. 2010, ApJ, 709, 670
Green, J. C., Wilkinson, E., & Morse, J. 2003, Proc. SPIE, 5164, 17
Green, J. C., et al. 2010, BAAS, 41, 501
Hebb, L., et al. 2009, ApJ, 693, 1920
Holmström, M., et al. 2008, Nature, 451, 970
Kochukhov, O. 2007, in Proc. Int. Conf., Physics of Magnetic Stars, ed. I. I. Romanyuk & D. O. Kudryavtsev, 109
Kupka, F., Piskunov, N., Ryabchikova, T. A., Stempels, H. C., & Weiss, W. W. 1999, A&AS, 138, 119
Lecavelier des Etangs, A., et al. 2010, A&A, in press (arXiv:1003.2206)
Li, S., Miller, N., Lin, D. N. C., & Fortney, J. J. 2010, Nature, 463, 1054
Morton, D. C. 1991, ApJS, 77, 119
Morton, D. C. 2000, ApJS, 130, 403
Osterman, S., et al. 2010, BAAS, 41, 502
Paczyński, B. 1971, ARA&A, 9, 183
Piskunov, N. E., Kupka, F., Ryabchikova, T. A., Weiss, W. W., & Jeffery, C. S. 1995, A&AS, 112, 525
Ryabchikova, T. A., Piskunov, N. E., Stempels, H. C., Kupka, F., & Weiss, W. W. 1999, Phys. Scr., T83, 162
Schneiter, E. M., Velazquez, P. F., Esquivel, A., & Raga, A. C. 2007, ApJ, 671, L57
Shulyak, D., Tsymbal, V., Ryabchikova, T., Stütz, Ch., & Weiss, W. W. 2004, A&A, 428, 993
Vidal-Madjar, A., et al. 2003, Nature, 422, 143
Vidal-Madjar, A., et al. 2004, ApJ, 604, L69
Vidal-Madjar, A., et al. 2008, ApJ, 676, L57
Yelle, R. V. 2004, Icarus, 170, 167